Effects of Humidity on Mycelium-Based Leather

Ashoka Karunarathne,[†] Günel Nabiyeva,[†] Christopher J. Rasmussen,[‡] Keven Alkhoury,[¶] Naila Assem,[‡] Jonathan Bauer,[‡] Shawn A. Chester,[¶] Alexei F. Khalizov,[§] and Gennady Y. Gor*,[†],[∥]

† Otto H. York Department of Chemical and Materials Engineering, New Jersey Institute of Technology, Newark, New Jersey 07102, United States

‡Bolt Threads Inc., San Francisco, California 94114, United States

¶Department of Mechanical Engineering, New Jersey Institute of Technology, Newark, New Jersey 07102, United States

§Department of Chemistry and Environmental Science, New Jersey Institute of Technology,
Newark, New Jersey 07102, United States

|| Department of Mechanical and Aerospace Engineering, Princeton University, Princeton,
New Jersey 08544, United States

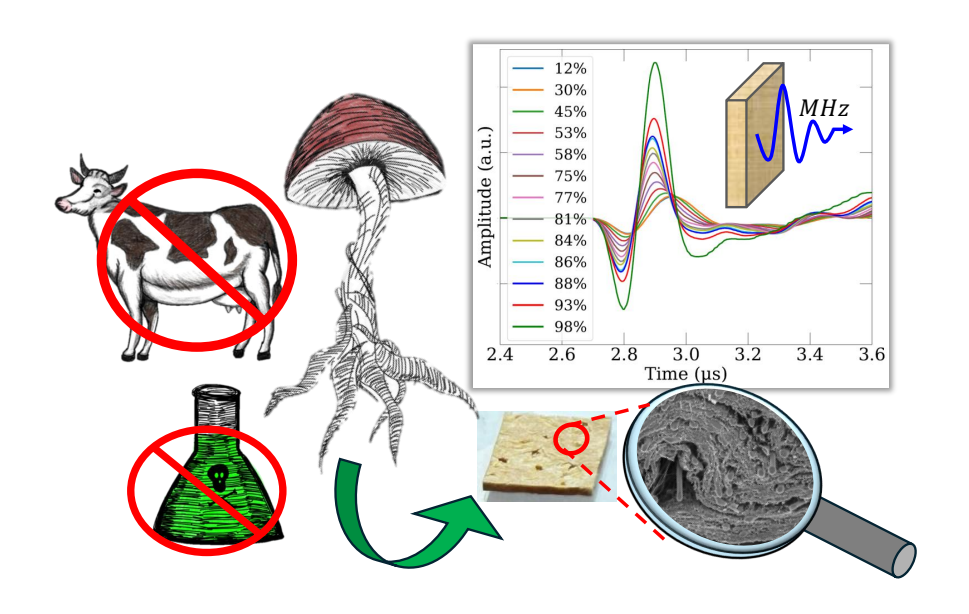
E-mail: gor@njit.edu

Abstract

Leather is a product which has been used for millennia. While it is a natural material, its production raises serious environmental and ethical concerns. To mitigate those, the engineering of sustainable bio-based leather substitutes has become a trend over the past few years. Among the bio-based materials, mycelium, the fungal "root" of a mushroom, is one of the promising alternatives to animal leather, as a material with tunable physico-mechanical properties. Understanding the effect of humidity on mycelium-based leather material properties is essential to the production of durable, competitive, and sustainable leather products. To this end, we measured the water sorption isotherms on several samples of mycelium-based leather materials and also investigated the effects of water sorption on their elastic properties. The ultrasonic pulse transmission method was used to measure the wave speed through the materials while measuring their adsorption isotherms at different humidity levels. Additionally, the material's properties were mechanically tested by performing uniaxial tensile tests under ambient and immersed conditions. An overall reduction of elastic moduli was observed during both absorption and immersion. The changes in the measured longitudinal modulus during water sorption reveal the changes in the elasticity of the test materials. The observed irreversible variation of the longitudinal modulus during the initial water adsorption can be related to the material production process and the presence of various additives that affect the mechanical properties of the leather materials. Our results should be of interest to material science experts developing a new generation of sustainable leather products.

Keywords: bio-based leather, water sorption, ultrasonic testing, elasticity, plasticisation

TOC Graphics



Introduction

Leather is a ubiquitous material that has been used by humans since prehistoric times. It is composed of type I collagen derived from animal hides and even today it is a globally demanded product due to its useful attributes, including strength, durability, flexibility, and aesthetics. However, the growing recognition of adverse environmental impacts associated with the manufacturing of animal-based leather propels the demand for bio-based alternatives, offering a sustainable solution to mitigate the ecological concerns in the leather industry. Traditional leather suffers from having a significant carbon footprint (both from its livestock source and tanning, the conversion of hides to leather), the use of hazardous chemicals during tanning, and ethical issues regarding the consumer use of animal-derived products. The most recent attempts in material science have been directed toward the rigorous engineering of natural leather substitutes in order to diminish the environmental burdens of the industry. 2,3,6-8 Among these substitutes, mycelium-based leather stands out as a promising and abundant alternative to non-sustainable products. 3,4,6,8-10

Mycelium can be considered the fungal "root" of the mushroom, and is composed of thread-like tubular filaments with a typical width of 2-10 μ m called hyphae. ^{3,10} The growth of tubular filament structure typically involves elongation of the tips and intermittent branching or merging with other hyphae. Thus, the process leads to the creation of a random network-like structure within the surrounding substrate which could be a broad range of waste biomaterials, such as wood. Colonization of the substrate by the fungi during growth causes inhomogeneities that alter the material properties, including compressive strength, bending strength, and thermal conductivity. ⁴ Hyphae typically comprises biopolymers, mainly proteins, chitin, and glucans which make the mycelium advantageous with remarkable mechanical and structural properties for the manufacturing of green materials. ^{3,6,11} Chitin is responsible for the structural stiffness with a tensile strength of 4000 MPa, while the ductility

of mycelium-based material is correlated to the lipids and proteins acting as bioplasticizers.⁶ The strength and elasticity of mycelium-based materials can be tailored for diverse applications while keeping the physical properties akin to genuine leather which aligns with the primary objective of the bio-based leather industry.

In the realm of mycelium-based materials, significant research has been conducted to explore various production methods and processing approaches, aiming to adjust their mechanical characteristics for diverse applications ^{6,12,13} Fredricks et al. ³ explored the various fabrication and treatment techniques to tune mechanical properties and densities to cater to different application requirements, where elastic moduli and strength could range from 0.02 to 3000 MPa and from 0.05 to 40 MPa, respectively for densities between 0.06 and $2\,\mathrm{g/cm^3}$. Tuning the properties of these materials mainly includes pressing, and the use of different substrates and additives. Appels et al. 14 studied mycelium-based composite foams grown on various substrates as well as pressing methods, reporting that the hot pressing resulted in more homogeneous composites with higher density and increased elastic modulus and flexural strength compared to unpressed or cold-pressed foams. Another study characterized the mechanical, thermal, and chemical properties of commercially available mushroom leather (MuSkin). ⁶ The simultaneous thermogravimetric analysis (TGA) and differential scanning calorimetry (DSC) show that mushroom leather exhibits thermal stability up to 250 °C which is similar to that of real leather $(271\,^{\circ}\mathrm{C})$. 6,15 It is mechanically robust with a tensile strength of 1.2 MPa and high ductility (101% strain at break), which is associated with the composition of chitin and proteins in the fibers. The fibers comprised 30% chitin and 70% proteins, as found by means of FTIR (Fourier Transform Infrared) analysis, and this balance can be adjusted by exposing the leather samples to different pH levels. While proteins exhibit a ductile and viscoelastic nature, chitin is known to contribute to the strength and hardness of fibers. Thus, by dissolving proteins in basic media and chitin in acidic media, the mechanical properties of mycelium-based leather can be tuned for different applications.⁶

It is critical to consider the water absorption characteristics of any natural leather alternatives, particularly the ability of these substitutes to exhibit reversible mechanical/elastic changes under varying relative humidities, mirroring the behavior observed in natural leather. For bovine leather, collagen molecules align in the strain direction during tanning, making it stiffer (increasing Young's modulus) due to the closer packing of molecules as well as fiber alignment. Increasing moisture content leads to better flexibility in the tanned leather samples since water absorption within collagen fibrils results in greater lateral spacing between collagen molecules. Rathinamoorthy et al. compared the moisture sorption and air permeability of mycelium sheets to cotton fabric, reporting a lower air permeability (25.77 cm³/sec/cm²) and water permeability (280.4 g/m²/day) due to their lower porosity (mycelium sheet: 53.08%, nonwoven fabric: 88.87%, knitted fabric: 79.21%). Also, mycelium sheets exhibited slower water absorption compared to cotton fabric. However, their study did not account for any potential changes in mechanical properties associated with water sorption.

Previous works mainly involved the tensile testing of mycelium-based materials to get access to the mechanical properties of the examined samples. ^{5,17,18} The tensile strength of leather needs to be high enough to survive article production (stitching, stretching, etc.) and consumer use. The elastic behavior is also a critical property of leather and other textiles, as it partially describes the hand-feel complexities and resiliency of the material. Both mechanical performance and dimensional and textural stability are a function of moisture content. In this study, we measured the water sorption isotherms on several samples of MyloTM, mycelium-based leather materials and investigated the impacts of water sorption on their elastic properties, by means of a novel technique: sorption-ultrasonics. ^{19–21} It is a non-destructive method to obtain the elastic properties of porous materials through wave propagation in the controlled environment. We monitored the wave speed traversing the mycelium leather samples exposed to different relative humidities and were able to exam-

ine the changes in mechanical properties during the adsorption and desorption processes. Additionally, we performed uniaxial tensile tests on the samples under ambient and water-immersed conditions to assess moisture impact on strength.

Materials and Methods

Test materials

In this study, select MyloTM mycelium-based leather samples were used to measure their adsorption isotherms and the ultrasonic wave speeds at different water saturations. The samples were produced by Bolt Thread's proprietary process, and are composed predominately of Ganoderma sessile mycelium, with fractions of cellulose-based fibrils, polymeric binder, and other additives. The material can be dyed or undyed. Generally, the process of producing MyloTM involves 4 steps: formulation, wetlay, dewatering, and hot pressing. Formulation involves the dispersion of the mycelium and fibers, as well as the incorporation of any "chemistry" or additives. The use of chemistry is necessary to achieve performance and aesthetic goals. The primary chemistry is a water-based polymer emulsion used as a binder that can optionally include crosslinking functionally. A secondary chemistry is used to improve softness and hand-feel. Other minor additives may include dye, stabilizers, process aids, and fiber conditioners. Note that the chemistry utilized by MyloTM can be synthetic or naturally derived, or a mix of both, depending on the version of the product. Once mixed, the slurry is then wetlaid and dewatered. The resulting "wet web" is then oven dried. While drying, the web can be dimensionally constrained, or unconstrained. Samples are allowed to dimensionally relax during the unconstrained drying and they typically shrink reducing their pore size and porosity. The samples after the drying process are labeled as "Web". Once optimal moisture content is reached, a hot press is employed to achieve a smooth surface and desired thickness. The hot pressed samples are labeled as "Crust". Optionally, a "rework" step can be performed by re-wetting and pressing a finished sample. The production process information and the physical properties of the samples examined in this work are provided in Table 1. Crust and Web samples with different formulation and production process are labeled as "Crust 1", "Crust 2", "Crust 3" and "Web 1". These crust samples were mainly used for adsorption-ultrasonic measurements, the web sample was used only for the sorption isotherm measurement. For other materials characterizations such as tensile test, dynamic mechanical analysis (DMA) and CT micro-tomography, samples analog to the above samples were used. These analog samples are labeled as "Crust 1A", "Crust 1B", etc. (analog to Crust 1) and they have similar materials properties of each respective Crust and Web samples. Square-shaped samples with each side of $1.000 \pm 0.032 \,\mathrm{cm}$ were cut from the bulk samples. The thickness of each crust sample was measured by a digital micrometer with an accuracy of $0.001 \,\mathrm{mm}$ (samples were sandwiched between two microscope glass slides to measure the uniform sample thickness). The dry densities were calculated using the sample masses measured after exposure to 2 Torr vacuum over 48 hours.

TABLE 1: Samples examined in this work. Sample Crust 1A is similar to Crust 1 and was used only for tensile testing. The surface of the Web 1 sample is not uniform so thickness value cannot be reliably reported. The web sample was used only for the isotherm measurements.

Designation	Binder Type	Drvo	Constrained	Hot	Dry Density	Thickness
	Crosslinking	Dye	Drying	Presses	(g/cm^3)	(mm)
Crust 1	No	None	Yes	2	0.900	0.759
Crust 1A	No	None	Yes	2	-	0.875
Crust 2	Yes	Black	Yes	2	0.741	1.134
Crust 3	Yes	Black	No	2	0.827	0.958
Web 1	Yes	Black	Yes	0	-	-

Material Characterization

To gain a comprehensive understanding of the material behavior of the leather samples, we conducted tensile tests on multiple specimens of each Crust 1A (3 specimens), Crust 2 (3

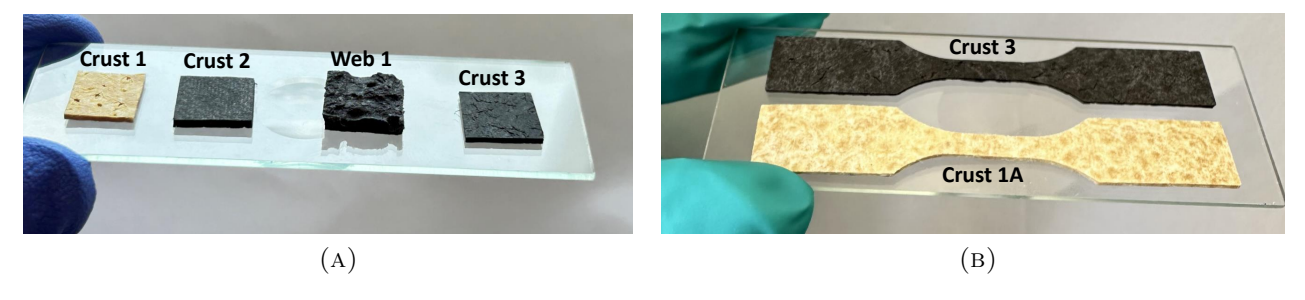


FIGURE 1: Test samples: (a) used for the adsorption isotherm and ultrasonic measurements and (b) used for tensile test. Note: the Web 1 sample is used only for the adsorption isotherm measurements. Ultrasonic experiments require monolithic samples with smooth surface, and Web sample does not meet these requirements.

specimens), and Crust 3 (4 specimens) under both ambient conditions and while immersed in water. Both ambient and water-immersed tensile tests were performed using an MTS Criterion Model 43 uniaxial testing machine under displacement control, and at a constant nominal strain rate of $\dot{\epsilon} = 1 \times 10^{-3} \, \mathrm{s}^{-1}$. Prior to the experiments, tensile dog bone samples (Fig. 1b) are extracted from the sheets using an ASTM D638-V cutting die. The nominal gauge section dimensions of our samples are 9.49 mm long, 3.18 mm wide. The ambient tests were carried out at a room temperature of 23 °C and 47% RH. The water-immersed tests were performed after allowing the sample to swell freely for over 24 hours at a water temperature of 23 °C. For the ambient tests, the leather samples were subjected to tensile forces within the elastic region up to a nominal strain of $\approx 0.8\%$, allowing the samples to be re-used for comparison without damaging them. For the water-immersed tests, the same leather samples were loaded until failure. The force is collected during the experiment using a 500N load cell (MTS Model LPB.502 D) and is later used to calculate the nominal stress based on the standard relation $\sigma = F/A_0$, where A_0 is the initial cross-sectional area which was measured for each sample. We note that there was no measurable change in the thickness due to swelling. The nominal strain was measured using the non-contact Digital Image Correlation (DIC) software Vic2D (Correlated Solutions) which is integrated with a digital camera (PointGrey GRAS-50S5M-C). Since the image analysis requires contrast, we apply white paint to the grip, where the sample is being held, and use it for strain measurement.

Dynamic mechanical analysis (DMA) provides valuable information about mechanical responses at different timescales and temperatures. These data can be compared to bovine hide leather, and used to guide product development so that mycelium-based leather is better at emulating bovine leather. DMA analysis was performed for single analog samples of each Crust 1 and Crust 2 samples in tension on a TA Instruments DMA Q800 with liquid nitrogen cooling accessory. Samples were cut with stencil and knife into strips 2 cm long and 5 mm wide. The samples were subjected to an oscillatory strain of 0.1% at a frequency of 1 Hz. The samples were tested in a temperature sweep from −100 °C to 150 °C, at a rate of 2 °C/min, in an atmosphere of dry nitrogen.

To better understand the pore size and structure, a CT micro-tomography study was commissioned by Bolt Threads, Inc. and performed by Micro Photonics, Inc. (Allentown, PA, USA). Though an earlier formulation of MyloTM was used for this study, we consider the results to be typical of samples examined in this work. Measurements were performed using a SkyScan 1272 (Bruker Corporation, Billerica, MA, USA) which allows for non-destructive imaging down to 0.35 μ m voxel size. For this work, a voxel size of 2.5 μ m was selected. The specimen was rotated 180° in 0.15° steps. Each exposure was 550 ms with a source voltage of 40 kV and a current of 150 μ A.

Adsorption-Ultrasonic Experimental Setup

Water sorption and ultrasonic measurements were conducted under humid air conditions, following Yurikov et al.¹⁹ and Ogbebor et al.²⁰ The relative humidity, RH = p/p_0 , is the ratio of the partial vapor pressure, p, to the saturation vapor pressure of water, p_0 , and the water saturation can be controlled by controlling the relative humidity. In this experiment,

a series of salt solutions were used to control the RH level ranging from 12% to 98%. In the experimental setup as shown in Fig. 2, the sample-transducer assembly, a sister sample, and the salt solution were placed inside a vacuum-tight container (AnaeroPackTM rectangular jar, Thermo ScientificTM R681001) held at ambient pressure. A 40 mm box fan was used inside the container to mix the vapor-air continuously and the humidity in the container was recorded using a VernierTM sensor with an accuracy of $\pm 2\%$ RH, a resolution of 0.01% RH. The container was placed inside a thermally insulated box (cooler box) with a finned shell-and-tube heat exchanger and a box fan. Temperature-controlled water was pumped through the heat exchanger by a FisherbrandTM IsotempTM bath circulator, model 6200 R20, with the temperature set to 27.00 ± 0.025 °C.

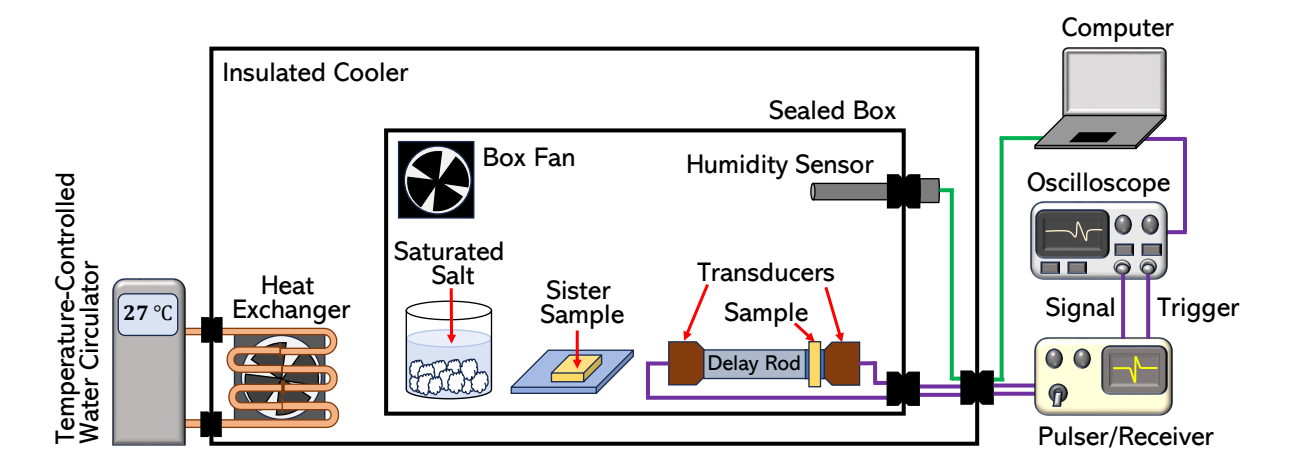


FIGURE 2: Schematic of adsorption-ultrasonic experimental setup. Thermally insulated sealed feed-throughs are used to insert the electrical cables into the sealed box to maintain a constant humidity level and temperature.

Ultrasonic Measurements

Ultrasonic pulse transmission technique is a widely used non-destructive experimental approach to probe the elastic properties of the materials by measuring both longitudinal (v_L) and shear (v_S) sound speeds through materials. ^{22–25} In this method, a transducer attached to one side of the test specimen transmits an ultrasonic pulse and the transducer attached to

the opposite side of the test specimen receives the pulse traveled through the test specimen. The time of flight can be determined by analyzing the time delay between the transmitting and receiving waveforms captured by the oscilloscope. Sound speed can be calculated using the measured time of flight Δt , and the path length of the sound through the sample (sample length or thickness) L, simply as $v = L/\Delta t$. The longitudinal modulus M, is related to the longitudinal wave speed and the material's density ρ , as

$$M = \rho v_{\rm L}^2. \tag{1}$$

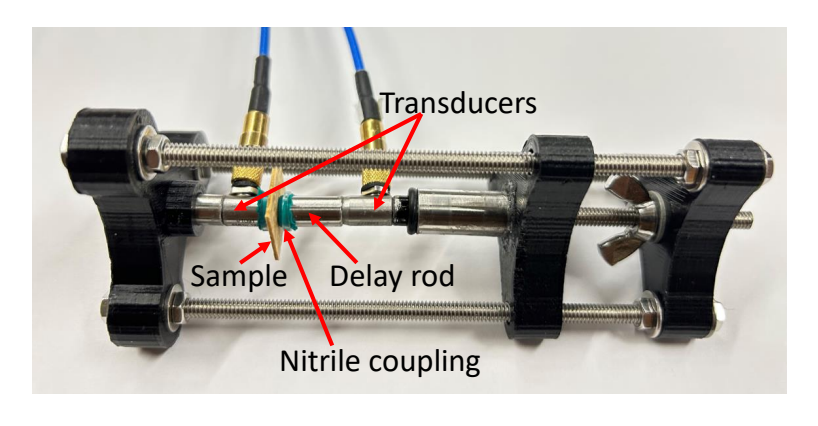
Unlike the standard tensile tests, which probe the Young's modulus of the material E, ultrasound propagation is related to different moduli. The primary (longitudinal) wave is related to the longitudinal modulus M, and the secondary (transverse) wave is related to the shear modulus G. While the Young's modulus quantifies the stiffness under uniaxial stress, the longitudinal modulus differs because it corresponds to the stiffness under uniaxial strain. For an isotropic material, which can be described in terms of two elastic constants, the three aforementioned moduli can be expressed in terms of the bulk modulus K and Poisson's ratio ν as

$$E = 3K(1 - 2\nu)$$
 $M = \frac{3K(1 - \nu)}{(1 + \nu)}$ $G = \frac{3K(1 - 2\nu)}{2(1 + \nu)}$. (2)

While the $Mylo^{TM}$ samples are strongly anisotropic composite materials, and Eq. 2 are not applicable, a correlation between E probed by uniaxial tensile testing and M from the ultrasonic experiments is expected.

For this study, the sample was sandwiched between longitudinal transducers with fundamental frequency 5 MHz and diameter 6.35 mm (manufactured by Olympus, part numbers V1091) by a custom-built clamp assembly as shown in Fig. 3a. Since the leather samples tend to deform with applied force, the separation between the transducers was kept constant such that the thickness of the sample was constant. A good contact between the sample and the

transducer surfaces is required for maximum pulse energy transmission through the material and a coupling medium is used at the transducer-sample interfaces to enhance the contact. For porous materials, the use of conventional fluid couplants is limited as they tend to diffuse through the materials. Therefore, thin nitrile rubber sheets were used as the coupling media between the leather sample and transducers. A Pulser/Receiver (JSR Ultrasonics brand DPR300), which generates negative spike pulses in 10 - 70 ns duration is connected to the transmitting transducer to generate ultrasonic pulses and transmit through the test material. The receiver transducer captures the ultrasonic pulse transmitted through the materials and converts it to an electrical signal. The pulser simultaneously sends a square wave trigger to the oscilloscope (Tekronix DPO2000B, 200 MHz, 1 GS/s, 1M record length) used to start monitoring the receiving transducer. Once the oscilloscope is triggered, defining t=0, the transmitted waveform was logged at a rate of 250 MHz. The oscilloscope was set to trigger at an amplitude of 1.4 V on the rising edge of the square trigger wave. A single measurement consisted of averaging 512 transmitted waveforms to improve the signal-to-noise ratio. Since the test samples are thin and the time of flight is close to the t=0 trigger point, a 12.95 mm long stainless steel delay rod with 6.35 mm diameter was used between the transmitting transducer and the sample so that the transmission waveform is well separated from the trigger point. In order to account for the additional time of flight through nitrile rubber and the delay rod, first, the pulse transmission through delay rod-nitrile-nitrile configuration was recorded without sample (reference waveform) (Fig. 3b). Then the wave form was recorded for rod-nitrile-sample-nitrile configuration (sample waveform) and the time difference between the reference waveform and the sample waveform was used as the flight time through the sample. The time of flight was determined using a standard cross-correlation technique where the transmitted waves are correlated with a reference waveform.



(A)

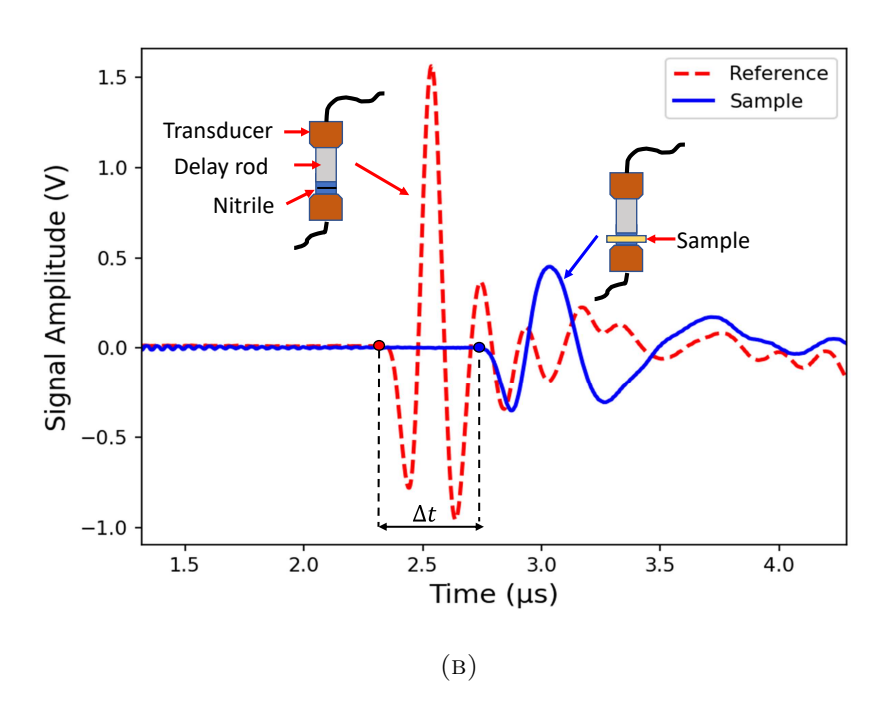


FIGURE 3: (a) Transducer-sample clamp assembly and (b) the longitudinal waveforms of the systems without and with sample.

Experimental Procedure

The equilibration time for the samples at each RH level was estimated to be 24 hours by monitoring mass change and the shift of the ultrasonic waveform with the time. After the RH equilibrated, the ultrasonic waveform was recorded on the sample attached to the transducers and the sister sample was weighted (Mettler AT261 DeltaRange analytical balance weighing capacity 205 g with a linearity of ± 0.15 mg), then the salt solution was replaced to adjust

to the next RH level and these steps were repeated to obtain the full adsorption isotherms. Dry mass, m_0 , and the dry elastic properties were measured in vacuum (2 Torr).

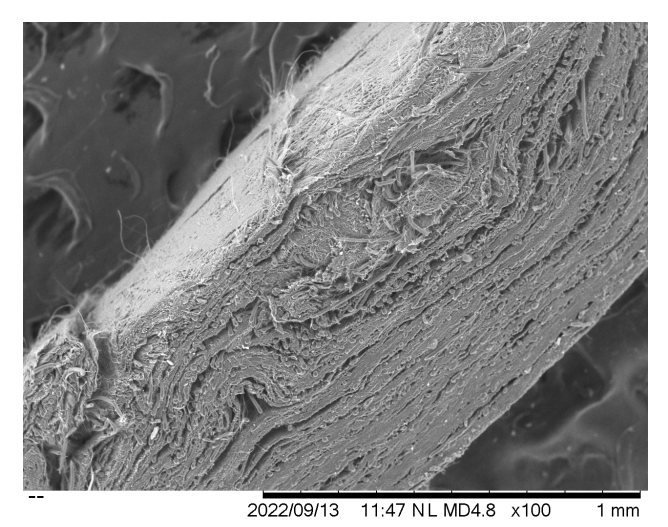
Results

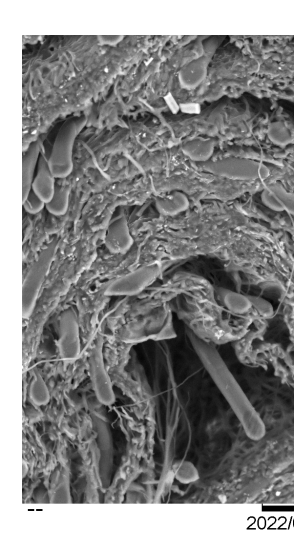
Material Properties

The wetlay process produces distinct layering of fibers. A cross-section of a typical MyloTM crust (similar in composition and construction to Crust 2) is given in Fig. 4a. At 100x magnification, both very fine hyphae and the coarse cellulose fibers are visible. Distinct layers, approximately 0.5 mm in thickness, are stacked with notable voids between. At high magnification (Fig. 4b), each layer is found to contain polymer-coated mycelium, with large cellulose fibers distributed both within and between layers. Examination of the microstructure confirms binder adhesion to mycelium and cellulose fibers, and confirms dispersion of the formulated components. It is also crucial in the diagnosis of defects, such as the large void captured in Fig. 4b.

The average pore size and porosity data obtained from the CT micro-tomography study of the samples with different production processes are given in the Table 2. As expected, the web samples have high porosity compared to hot pressed samples, indicating that hot pressing results in a reduction of porosity due to the application of pressure and temperature. The measured porosity values of hot pressed samples reveal a direct correlation between the porosity and the drying conditions. Samples dried with dimensional constraints show higher porosity of $\sim 55\%$ compared to samples dried without constraints ($\sim 48\%$). This implies that the sample shrinkage occurring during unconstrained drying leads to a reduction in pore size and porosity.

Fig. 5 compares two different versions of Mylo $^{\rm TM}$ over a temperature sweep from $-100\,^{\circ}{\rm C}$





100x.png 100x.png 500x.png 500x.png (a) (B)

FIGURE 4: (a) Micrograph of a Mylo cross-section. Acquired with Hitachi TM3000II tabletop SEM. (b) Zoom of figure above, 500X magnification on a large void feature.

Table 2: Average pore size and porosity present in web and pressed samples.

Designation	Web 1A	Web 1B	Crust 1B	Crust 3A	Crust 3B	Crust 1C
Hot presses	No	No	Yes	Yes	Yes	Yes
Constrained drying	n/a	n/a	Yes	No	No	Yes
Avg. pore size (µm)	64.3	113.3	8.56	8.42	8.04	8.66
Porosity (%)	67.2	65.3	55.8	47.9	47.8	53.8

to 150 °C. A key metric is the position of the glass-transition temperature $(T_{\rm g})$, below which the material may begin to feel stiff and "plastic-like". In the Fig. 5a, the formulation exhibits a $T_{\rm g}$ of -17.77 °C (as assessed by the temperature of maximum peak of tan δ), while the Fig. 5b is 3.58 °C. This is primarily attributed to the bulk $T_{\rm g}$ of the selected binder chemistry, as it forms a semi-continuous phase for the fibers to become embed in. In the presented case, $T_{\rm g}$ is lower for the Crust 1-analog due to the inclusion of a plasticizer in the formulation. Another feature of these data is the aptly named "leathery region," the region where of storage modulus between $T_{\rm g}$ and the rubbery-plateau. This region is described as "tough but flexible," and product design aims to keep the region in temperature ranges that are expected to be encountered in routine use. The formulation of Crust 1 performs better

in this regard, with a wide leathery region from $-37.5\,^{\circ}\text{C}$ to $50\,^{\circ}\text{C}$. The positions and widths of the peaks for both samples are close to that for the bovine leather from the literature, e.g. by Jeyapalina et al.²⁶

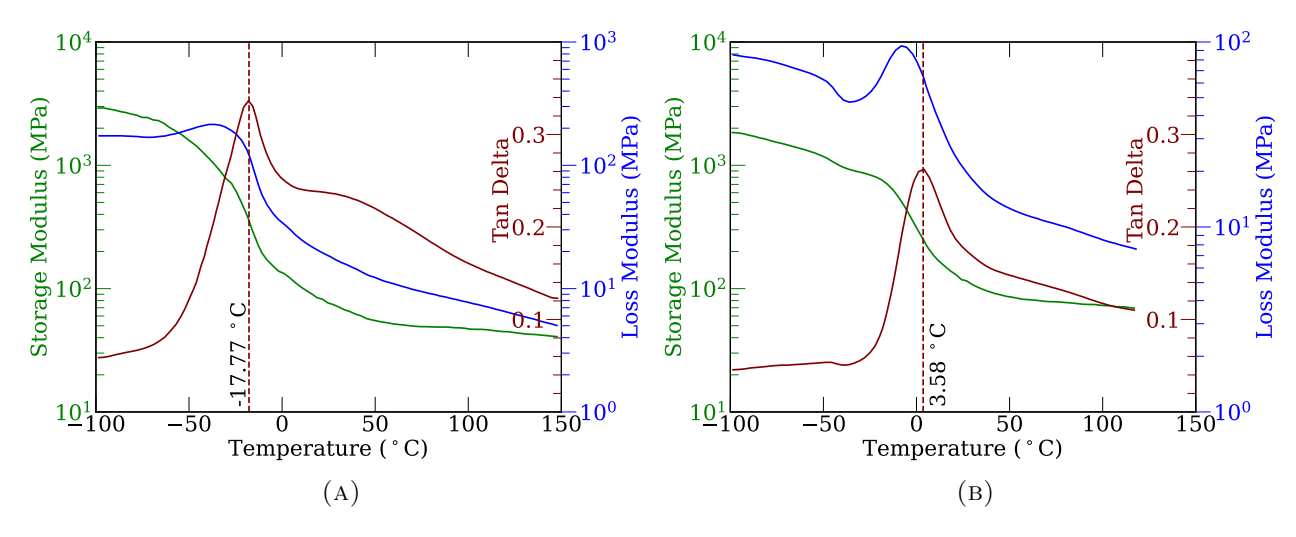


FIGURE 5: DMA temperature sweep measured in a dry nitrogen atmosphere, with (a) Crust 1-analog and (b) Crust 2-analog.

Elastic Properties in Air and in Water

Fig. 6a shows the results of the tensile tests – stress-strain curves for the Crust 2 sample at ambient conditions (dash lines) and Crust 1A, Crust 2, and Crust 3 samples immersed in water. Compared to immersed samples, samples at ambient conditions show a high stiffness followed by a high ultimate tensile strength of 4 MPa. Immersed samples clearly exhibit less strength upon deformation, and the ultimate tensile strength of the immersed samples has reduced by > 50% compared to the ambient samples. Young's modulus, a measure of material stiffness, can be determined from the slope of the stress-strain curve within its elastic deformation region. Fig. 6b shows the stress-strain curves with linear curve fittings of the ambient and immersed samples within their elastic region up to 0.01 of nominal strain. Notably, all three samples (Crust 1A, Crust 2, Crust 3) follow similar behavior when submerged in water. The samples under ambient conditions have Young's moduli of 124.78

MPa, 90.46 MPa, and 47.70 MPa, while the samples immersed in water experience an average reduction of 86 %, resulting in Young's moduli of 13.88 MPa, 13.51 MPa and 7.49 MPa for Crust 1A, Crust 2, and Crust 3, respectively.

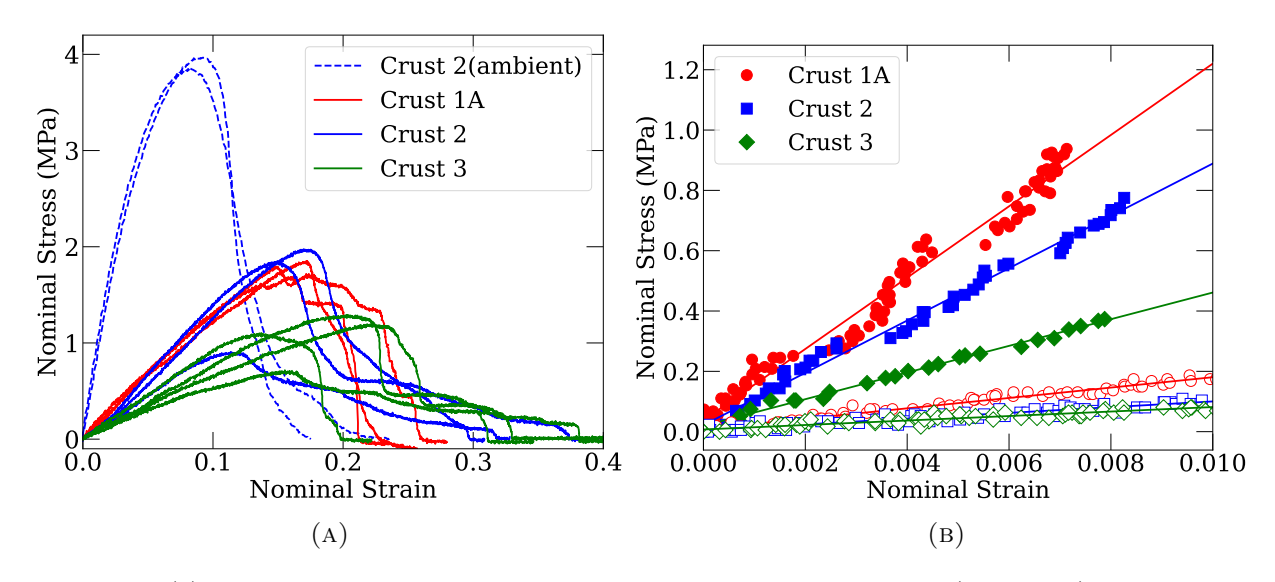


FIGURE 6: (a) Stress-strain curves for Crust 2 sample at ambient conditions (dash lines) and Crust 1A, Crust 2, and Crust 3 samples immersed in water. (b) Stress-strain curves for ambient (filled markers) and immersed (empty markers) Crust 1A, Crust 2, and Crust 3 samples at the elastic region, used for the Young's modulus calculations.

Water Sorption Isotherms

The water sorption isotherms of Crust 1, Crust 2, Crust 3 and Web 1 samples are shown in Fig. 7. All the samples show isotherms with 15%-25% water mass adsorption relative to the dry mass at P=2 Torr. The small hysteresis observed for all four samples, can be attributed to uncertainty in the experimental measurements for samples Crust 1 and Crust 3, but is more pronounced for samples Crust 2 and Web 1, and resembles the H4 hysteresis, observed during physisorption of vapors in some microporous materials.²⁷

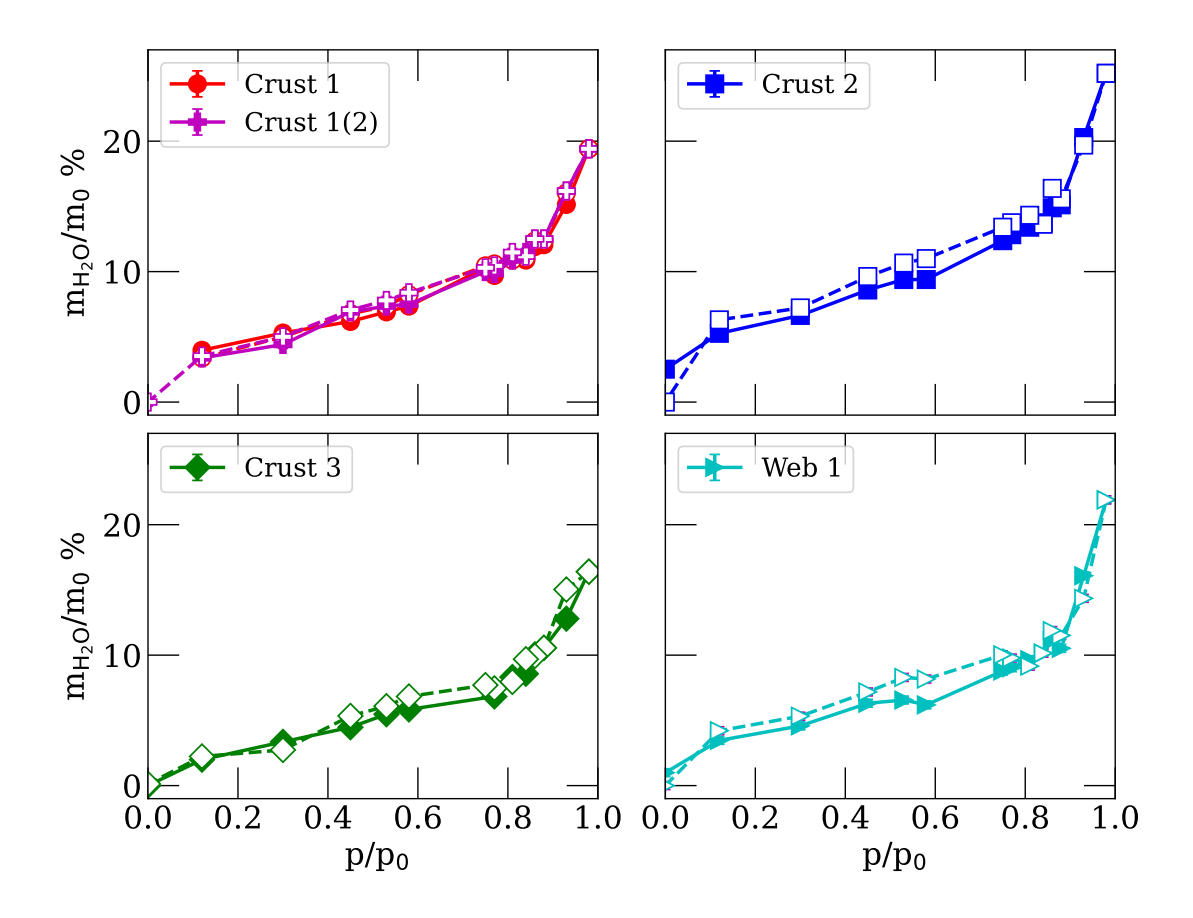


FIGURE 7: Water sorption isotherms, mass of water adsorbed $m_{\rm H_2O}$, relative to the dry mass m_0 , of each sample at the vacuum P=2 Torr. Magenta color lines (Crust 1(2)) represent the second adsorption/desorption path of Crust 1 sample. Solid lines with filled markers: adsorption and dashed lines with empty markers: desorption.

Elastic Properties from Sorption-Ultrasonic Measurements

Analysis of the ultrasonic waveforms recorded at different RH provide the information of the time of flight, which can be converted to the wave speed (the thickness of the samples is assumed unaffected). Fig. 8a shows the variation of the longitudinal wave speed as a function of relative humidity for the three samples used in ultrasonic tests. Eq. 1 allows one to calculate the corresponding longitudinal modulus M. The density in Eq. 1 increases with RH as a result of adsorption, but the density change is less pronounced compared to

the change in the velocity. Therefore, the shape of the moduli dependence on RH, shown in Fig. 8b is similar to the shape of the velocity plots.

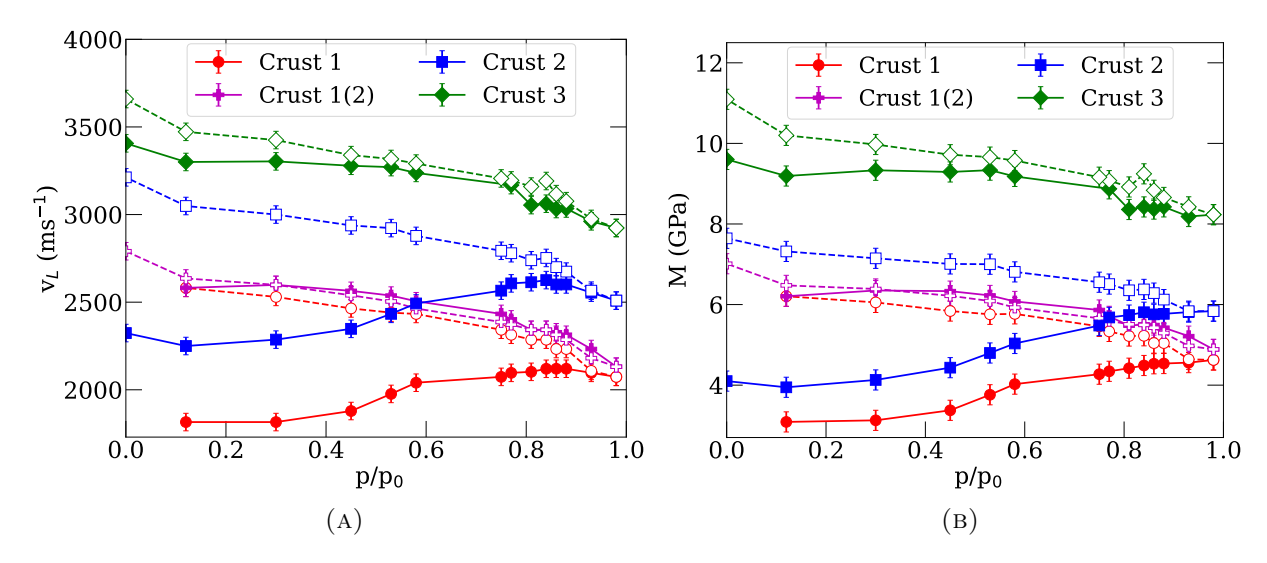


FIGURE 8: Variations in (a) longitudinal wave speed and (b) longitudinal modulus with the water adsorption and desorption. Magenta color lines (Crust 1(2)) represent the second adsorption/desorption path of Crust 1 sample. Solid lines with filled markers correspond to adsorption and dashed lines with empty markers correspond to desorption.

Sample Crust 3 showed a monotonic, and almost reversible dependence of the longitudinal modulus on relative humidity: decrease during adsorption, followed by the increase during the desorption. Samples Crust 1 and Crust 2, however showed different behavior – the moduli of both increased during adsorption, and increased even further with desorption. As a result, the modulus probed after the adsorption-desorption cycle appeared noticeably higher than the modulus of as-received samples. To clarify the origin of this irreversibility an additional adsorption-desorption cycle was performed on sample Crust 1. The modulus calculated from this second cycle coincided with the modulus measured during the desorption in the first cycle. The moduli measured at the lowest and highest RH, before and after adsorption-desorption cycles, are summarized in Table 3 along with the moduli measured from tensile testing.

Table 3: Summary of elastic moduli from tensile testing and ultrasonic measurements. E is given in MPa, M is in GPa. (* as received)

Designation	E (dry)	E (immersed)	M (initial)*	M (RH 98%)	M (dried)
Crust 1	-	-	3.09	4.63	7.01
Crust 1A	124.78	13.88	-	-	-
Crust 2	90.46	13.51	4.10	5.84	7.64
Crust 3	47.40	7.49	9.60	8.23	11.1

Discussion

Vapor Sorption

The shape of the isotherms, the amount adsorbed, and shape of the hysteresis measured on MyloTM samples, are similar to those obtained for water on various biopolymers, in particular polysacharides, chitin^{28–30} and cellulose, ^{31,32} which are both constituents of MyloTM. Since the amount of adsorbed water at maximum RH is only 15%-25%, the porosity of the samples (48-67%) is not getting filled with water, and most of the water adsorbs in the polymer constituents of the samples. This is consistent with the pore sizes of 10 μ m observed in the CT-scan experiments. Note that the amount adsorbed and the shape of the isotherm is similar to the adsorption isotherm on natural leather, ³³ see comparison in Fig. 9a.

Although we refer to the measured data as "adsorption" isotherms, similarly to many other biopolymers, this is absorption, rather than adsorption³⁴ – water molecules penetrate between the polymer chains of various MyloTM constituents. For simple polymer-solvent pairs³⁵ this process can be described within the Flory-Huggins theory, ³⁶ which relates the activity of the solvent a_s (RH) to its volume fraction v_s and volume fraction of the polymer $v_p = 1 - v_s$ as

$$\ln a_{\rm s} = \ln v_{\rm s} + v_{\rm p} + \chi v_{\rm p}^2 \tag{3}$$

The Flory-Huggins parameter χ here represents some effective value for all polymer constituents of MyloTM. It can be calculated from the sorption at the maximum activity, which

is $a_{\text{max}} = 0.98$ in our experiments. Therefore, we have

$$\chi = \frac{\ln a_{\text{max}} - (\ln v_{\text{s}}(a_{\text{max}}) + v_{\text{p}}(a_{\text{max}}))}{v_{\text{p}}(a_{\text{max}})^2}$$
(4)

The volume fraction of the solvent in Eqs. 3 and 4 can be related to the measured relative mass adsorbed $f \equiv m_{\rm H_2O}/m_0$ as

$$v_{\rm s} = \frac{f}{f + \rho_{\rm H_2O}/\rho_{\rm D}},\tag{5}$$

where $\rho_{\rm H_2O}$ and $\rho_{\rm p}$ are the densities of water and the polymer constituents of the MyloTM samples. The density of the polymer is related to the measured density of the porous samples ρ_0 through the porosity ϕ

$$\rho_{\rm p} = \frac{\rho_0}{1 - \phi}.\tag{6}$$

The estimated porosity values from CT measurements are given in the Table 2.

The resulting plots for samples Crust 1, Crust 2, and Crust 3, are shown in Fig. 9b, with Flory-Huggins parameters calculated from Eq. 4 $\chi=1.02,\,0.99,\,$ and 1.21, respectively. Given the complexity of the materials structure, the agreement with the sorption based on the Flory-Huggins theory can be considered satisfactory – at activities of the solvent above 0.7, the mean absolute percentage error for activities predicted using Eq. 3 are only 2% for Crust 1 and 2, and 8% for Crust 3. However, irrespective of the value of the Flory-Huggins parameter, Eq. 3 predicts concave curve, while the initial part of the adsorption isotherm is convex. This concave shape of sorption isotherms is well-documented for water in biopolymers, and is typically attributed to the glassy state of a polymer at low water concentration. $^{37-39}$ This is certainly the case for cellulose, shown in Figure 9a, and it likely applies to the MyloTM samples which are in the "leathery region", just slightly above $T_{\rm g}$. Theoretical representation of such concave isotherms requires several additional parameters, 37 and is

beyond the basic discussion given here. Note that the proximity to the $T_{\rm g}$ is likely to be the reason for the the sorption isotherms hysteresis, as it is typically observed in glassy polymers. $^{40-42}$

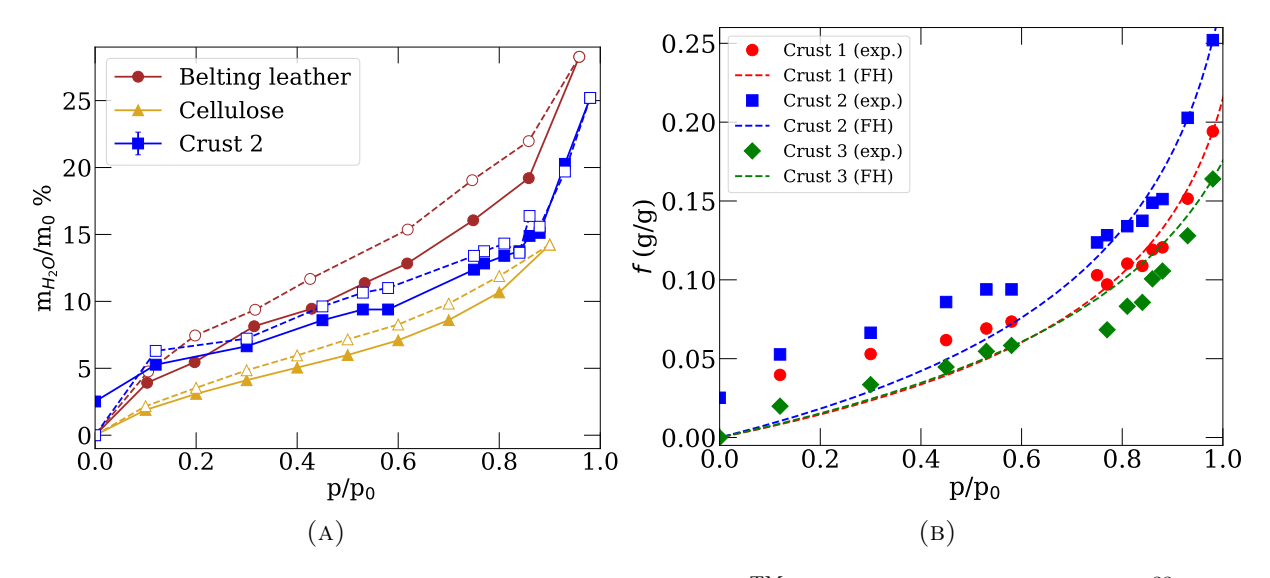


FIGURE 9: (a) Comparison of water sorption isotherm on MyloTM sample and on natural leather ³³ and on cellulose. ³² For each of the series solid lines with filled markers show adsorption, and dashed lines with empty markers show desorption. (b) Water sorption isotherms, mass of water adsorbed: measured experimentally and calculated using the Flory-Huggins equation

Elastic Properties

The trend observed for the longitudinal modulus of the sample Crust 3 as a function of RH is expected, and is consistent with the change of the Young's modulus observed in dry vs immersed sample. Favorable interaction of water with polymer constituents of MyloTM cause their plasticization, so the modulus decreases with the increase of the amount of adsorbed water. The same trend is observed for the second adsorption-desorption cycle of the sample Crust 1. The change of the modulus measured in the first cycle for Crust 1 and Crust 2 cannot be interpreted based on the simple polymer physics.

During the initial water adsorption path, Crust 1 sample shows a irreversible material stiffening followed by a further stiffening during the desorption path. After that, this sample

demonstrates a reversible material softening and stiffening trend during the second adsorption and desorption paths, respectively. Crust 2 sample exhibits the same trend of irreversible material stiffening during the initial water vapor adsorption. The observed irreversible material stiffening during the initial adsorption path reveals a permanent change of the material upon exposure to the water vapor for the first time. This behavior can be related to the mechanical history of the samples – both Crust 1 and Crust 2 were dried after their wetlay by constraining the web on a rigid polypropylene mesh, while Crust 3 was allowed to dry unconstrained. A dimensional change of about 5% was observed after this unconstrained drying, indicating some relaxation of the previously swollen fiber network. Therefore, by preventing this relaxation upon drying, unintentional internal stresses may be developed in those constrained samples. Upon rewetting, these residual internal stresses are allowed to relax by reducing the pore size and porosity (shrinkage). Reduction of pore size and porosity result in observed permanent increase of longitudinal modulus. Lastly, it is important to note that after the initial cycles, sample Crust 1 (and presumably Crust 2 as well) stops showing the anomalies, consistent with this hypothesis of relaxation upon full hydration.

Conclusion

Finding sustainable replacements for environmentally impactful products continues to be a challenge. Consumer preference, acceptable performance, cost, and availability define the success of such products. The quantitative understanding of qualitative consumer preference helps development and adoption of such products. The leather industry has evolved with and adopted metrics around consumer preference: fullness, handfeel, drape, and breaking are all multi-variable functions of mechanical and physical properties, and lack any direct mapping to such. Detailed mechanical characterization of such products are rare.

In the current work we offered a more complete understanding of how ambient moisture

gets sorbed by MyloTM mycelium-based leather, and how water sorption affects mechanical properties of this material, quantified by longitudinal modulus. Specifically, we performed detailed characterization of several MyloTM samples and measured the water vapor sorption isotherms. The amount of water sorbed on MyloTM samples as a function of relative humidity suggest that there is no adsorption by the porous structure, but it is absorption in the polymer constituents. Sorption isotherms are similar to other natural polymers, such as chitosan and cellulose, and are also comparable to sorption isotherms on natural leather.

We studied the effects of vapor sorption on mechanical properties of the MyloTM samples. Although tensile tests of samples immersed in water can give some idea of change of mechanical properties, complete immersion is not relevant to the conditions at which the product is used. Our unique experimental setup allowed us to measure the elastic properties of the samples during stepwise sorption process. We observed significant changes in longitudinal moduli of the samples as a function of relative humidity. Ultrasonic measurements not only allowed to observe the change of the elastic properties (longitudinal modulus), but also helped identifying the dependence of the mechanical properties of the samples on their fabrication history (unconstrained vs constrained drying). The former showed the decrease of the modulus with the increase of relative humidity – a typical plasticisation effect. While the latter showed the opposite trend on the first cycle of water sorption. These results demonstrate the role of the production process on the properties of the final product with respect to response to humidity.

Overall, our results directly relate to the user's expectation of acceptable form and function during typical use. A plausible mechanism for the interaction of water with MyloTM is presented, and sorption characteristics of MyloTM are shown to be similar to bovine leather at nominal humidity values. Novel and complex products like MyloTM will continue to require study to achieve required performance and consumer acceptance within the constrains of source materials and product life-cycle consideration.

Acknowledgment

G.Y.G., A.F.K. and A.K. thank the support from NSF CBET-2128679 grant. The work of G.Y.G. and G.N. was also supported by NSF CBET-1944495 grant. S.A.C. acknowledges partial support from NSF CMMI-1751520 grant. The opinions, findings, and conclusions, or recommendations expressed are those of the author(s) and do not necessarily reflect the views of the National Science Foundation. C.J.R. is employed by and receives financial compensation from Bolt Threads Inc., the owner of the MyloTM product and brand.

Associated content

Supporting Information

The Supporting Information is available free of charge at https://pubs.acs.org/doi/...

The tabulated experimental data plotted in Figures 5-8: geometrical parameters, adsorption and ultrasonic data, tensile test data, dynamic mechanical analysis data (ZIP)

References

- (1) Kelly, S. J. R.; Weinkamer, R.; Bertinetti, L.; Edmonds, R. L.; Sizeland, K. H.; Wells, H. C.; Fratzl, P.; Haverkamp, R. G. Effect of collagen packing and moisture content on leather stiffness. *Journal of the Mechanical Behavior of Biomedical Materials* 2019, 90, 1–10.
- (2) Ziegler, A. R.; Bajwa, S. G.; Holt, G. A.; McIntyre, G.; Bajwa, D. S. Evaluation of physico-mechanical properties of mycelium reinforced green biocomposites made from cellulosic fibers. Applied engineering in agriculture 2016, 32, 931–938.
- (3) Fredricks, J. L.; Jimenez, A. M.; Grandgeorge, P.; Meidl, R.; Law, E.; Fan, J.; Roumeli, E. Hierarchical biopolymer-based materials and composites. *Journal of Polymer Science* 2023, 1–48.
- (4) Muiruri, J. K.; Chuan Yeo, J. C.; Zhu, Q.; Ye, E.; Loh, X. J.; Li, Z. Sustainable mycelium-bound biocomposites: design strategies, materials properties, and emerging applications. ACS Sustainable Chemistry & Engineering 2023, 11, 6801–6821.
- (5) Meyer, M.; Dietrich, S.; Schulz, H.; Mondschein, A. Comparison of the technical performance of leather, artificial leather, and trendy alternatives. *Coatings* **2021**, *11*, 226.
- (6) Bustillos, J.; Loganathan, A.; Agrawal, R.; Gonzalez, B. A.; Perez, M. G.; Ramaswamy, S.; Boesl, B.; Agarwal, A. Uncovering the mechanical, thermal, and chemical characteristics of biodegradable mushroom leather with intrinsic antifungal and antibacterial properties. ACS Applied Bio Materials 2020, 3, 3145–3156.
- (7) Raman, J.; Kim, D.-S.; Kim, H.-S.; Oh, D.-S.; Shin, H.-J. Mycofabrication of mycelium-based leather from Brown-rot fungi. *Journal of Fungi* **2022**, *8*, 317.

- (8) Manan, S.; Atta, O. M.; Shahzad, A.; Ul-Islam, M.; Ullah, M. W.; Yang, G. Fungal Biopolymers and Biocomposites: Prospects and Avenues; Springer, 2022; pp 147–168.
- (9) Williams, E.; Cenian, K.; Golsteijn, L.; Morris, B.; Scullin, M. L. Life cycle assessment of MycoWorks' ReishiTM: the first low-carbon and biodegradable alternative leather. Environmental Sciences Europe **2022**, 34, 120.
- (10) Elsacker, E.; Zhang, M.; Dade-Robertson, M. Fungal Engineered Living Materials: The Viability of Pure Mycelium Materials with Self-Healing Functionalities. Advanced Functional Materials 2023, 2301875.
- (11) Haneef, M.; Ceseracciu, L.; Canale, C.; Bayer, I. S.; Heredia-Guerrero, J. A.; Athanassiou, A. Advanced materials from fungal mycelium: fabrication and tuning of physical properties. *Scientific reports* **2017**, *7*, 1–11.
- (12) Yang, L.; Park, D.; Qin, Z. Material function of mycelium-based bio-composite: A review. Frontiers in Materials 2021, 374.
- (13) Gandia, A.; van den Brandhof, J. G.; Appels, F. V. W.; Jones, M. P. Flexible fungal materials: shaping the future. *Trends in Biotechnology* **2021**, *39*, 1321–1331.
- (14) Appels, F. V. W.; Camere, S.; Montalti, M.; Karana, E.; Jansen, K. M. B.; Dijksterhuis, J.; Krijgsheld, P.; Wösten, H. A. B. Fabrication factors influencing mechanical, moisture-and water-related properties of mycelium-based composites. *Materials & Design* **2019**, *161*, 64–71.
- (15) Półka, M. Leather thermal and environmental parameters in fire conditions. Sustainability 2019, 11, 6452.
- (16) Rathinamoorthy, R.; Bharathi, T. S.; Snehaa, M.; Swetha, C. Structural and Chemical

- Characterization of Mycelium Sheets Developed from Penicillium Camemberti. *Journal* of Polymers and the Environment 2023, 1–14.
- (17) Pylkkänen, R.; Werner, D.; Bishoyi, A.; Weil, D.; Scoppola, E.; Wagermaier, W.; Safeer, A.; Bahri, S.; Baldus, M.; Paananen, A., et al. The complex structure of Fomes fomentarius represents an architectural design for high-performance ultralightweight materials. *Science advances* **2023**, *9*, eade5417.
- (18) Asadollahzadeh, M.; Mahboubi, A.; Taherzadeh, M. J.; Åkesson, D.; Lennartsson, P. R. Application of fungal biomass for the development of new polylactic acid-based biocomposites. *Polymers* 2022, 14, 1738.
- (19) Yurikov, A.; Lebedev, M.; Gor, G. Y.; Gurevich, B. Sorption-induced deformation and elastic weakening of Bentheim sandstone. *Journal of Geophysical Research: Solid Earth* **2018**, *123*, 8589–8601.
- (20) Ogbebor, J.; Valenza, J. J.; Ravikovitch, P. I.; Karunarathne, A.; Muraro, G.; Lebedev, M.; Gurevich, B.; Khalizov, A. F.; Gor, G. Y. Ultrasonic study of water adsorbed in nanoporous glasses. *Physical Review E* **2023**, *108*, 024802.
- (21) Wu, R.; Selvadurai, P. A.; Li, Y.; Sun, Y.; Leith, K.; Loew, S. Laboratory acousto-mechanical study into moisture-induced changes of elastic properties in intact granite. International Journal of Rock Mechanics and Mining Sciences 2023, 170, 105511.
- (22) Brown, A. E. Rationale and summary of methods for determining ultrasonic properties of materials at Lawrence Livermore National Laboratory; 1995.
- (23) Asay, J. R.; Lamberson, D. L.; Guenther, A. H. Ultrasonic Technique for Determining Sound-Velocity Changes in High-Loss Materials. *The Journal of the Acoustical Society of America* **1969**, *45*, 566–571.

- (24) Kohlhauser, C.; Hellmich, C. Ultrasonic contact pulse transmission for elastic wave velocity and stiffness determination: Influence of specimen geometry and porosity. *Engineering Structures* **2013**, *47*, 115–133.
- (25) Pantea, C.; Rickel, D. G.; Migliori, A.; Leisure, R. G.; Zhang, J.; Zhao, Y.; El-Khatib, S.; Li, B. Digital ultrasonic pulse-echo overlap system and algorithm for unambiguous determination of pulse transit time. *Review of Scientific Instruments* **2005**, 76.
- (26) Jeyapalina, S.; Attenburrow, G. E.; Covington, A. D. Dynamic mechanical thermal analysis (DMTA) of leather part 1: effect of tanning agent on the glass transition temperature of collagen. *Journal of the Society of Leather Technologists and Chemists* **2007**, *91*, 236–242.
- (27) Thommes, M.; Kaneko, K.; Neimark, A. V.; Olivier, J. P.; Rodriguez-Reinoso, F.; Rouquerol, J.; Sing, K. S. W. Physisorption of gases, with special reference to the evaluation of surface area and pore size distribution (IUPAC Technical Report). *Pure and applied chemistry* **2015**, *87*, 1051–1069.
- (28) Chalykh, A. E.; Petrova, T. F.; Khasbiullin, R. R.; Ozerin, A. N. Water sorption on and water diffusion in chitin and chitosan. *Polymer Science Series A* **2014**, *56*, 614–622.
- (29) Aguirre-Loredo, R. Y.; Rodríguez-Hernández, A. I.; Morales-Sánchez, E.; Gómez-Aldapa, C. A.; Velazquez, G. Effect of equilibrium moisture content on barrier, mechanical and thermal properties of chitosan films. *Food chemistry* **2016**, *196*, 560–566.
- (30) Aguirre-Loredo, R. Y.; Velazquez, G.; Guadarrama-Lezama, A. Y.; Viveros-Contreras, R.; Castaño, J. Water adsorption thermodynamical analysis and mechanical characterization of chitosan and polyvinyl alcohol-based films. *Journal of Polymers and the Environment* **2022**, 1–13.

- (31) Smith, S. E. The sorption of water vapor by high polymers. *Journal of the American Chemical Society* **1947**, *69*, 646–651.
- (32) Salmén, L.; Larsson, P. A. On the origin of sorption hysteresis in cellulosic materials.

 Carbohydrate polymers 2018, 182, 15–20.
- (33) Kanagy, J. R. Adsorption of water vapor by untanned hide and various leathers at 100 F. Journal of American Leather Chemists Association 1947, 42, 98.
- (34) Gor, G. Y.; Scherer, G. W.; Stone, H. A. Bacterial Spores Respond to Humidity Similarly to Hydrogels. *Proceedings of the National Academy of Sciences* **2024**, *121*, e2320763121.
- (35) Favre, E.; Schaetzel, P.; Nguygen, Q.; Clement, R.; Neel, J. Sorption, diffusion and vapor permeation of various penetrants through dense poly (dimethylsiloxane) membranes: a transport analysis. *Journal of Membrane Science* **1994**, *92*, 169–184.
- (36) Gedde, U. W.; Hedenqvist, M. S. Fundamental polymer science; Springer, 2019.
- (37) Vrentas, J. S.; Vrentas, C. M. Sorption in glassy polymers. *Macromolecules* **1991**, *24*, 2404–2412.
- (38) Hancock, B. C.; Zografi, G. The use of solution theories for predicting water vapor absorption by amorphous pharmaceutical solids: A test of the Flory–Huggins and Vrentas models. *Pharmaceutical research* **1993**, *10*, 1262–1267.
- (39) Hill, C.; Beck, G. On the applicability of the Flory–Huggins and Vrentas models for describing the sorption isotherms of wood. *International Wood Products Journal* **2017**, 8, 50–55.
- (40) Fleming, G. K.; Koros, W. J. Dilation of polymers by sorption of carbon dioxide at

- elevated pressures. 1. Silicone rubber and unconditioned polycarbonate. *Macromolecules* **1986**, *19*, 2285–2291.
- (41) Doghieri, F.; Sarti, G. C. Nonequilibrium lattice fluids: a predictive model for the solubility in glassy polymers. *Macromolecules* **1996**, *29*, 7885–7896.
- (42) Vrentas, J. S.; Vrentas, C. M. Hysteresis effects for sorption in glassy polymers. *Macro-molecules* **1996**, *29*, 4391–4396.